

Velocity dispersion measurements of dwarf galaxies in the Coma cluster - implications for the structure of the fundamental plane

A.M. Cody^{1,2}, D. Carter³, T.J. Bridges^{1,4}, B. Mobasher^{5,7}, B.M. Poggianti⁶.

¹ *Anglo-Australian Observatory, PO Box 296, Epping NSW 1710, Australia.*

² *Astronomy Department, Caltech, MC 105-24, 1201 East California Blvd, Pasadena CA 91125, USA.*

³ *Astrophysics Research Institute, Liverpool John Moores University, Twelve Quays House, Egerton Wharf, Birkenhead CH41 1LD, UK.*

⁴ *Department of Physics, Engineering Physics, and Astronomy, Queen's University, Kingston, Ontario, K7L 3N6, Canada.*

⁵ *University of California, Riverside, 900 University Ave., Riverside, CA 92521, USA.*

⁶ *Osservatorio Astronomico di INAF, Università di Padova, Vicolo dell'Osservatorio 5, I-35122 Padova, Italy.*

⁷ *Visiting Astronomer, Kitt Peak National Observatory, National Optical Astronomy Observatories, which is operated by the Association of Universities for Research in Astronomy, Inc. (AURA) under cooperative agreement with the National Science Foundation*

Accepted Received ... ; in original form ...

ABSTRACT

We present intermediate-resolution spectroscopic data for a set of dwarf and giant galaxies in the Coma Cluster, with $-20.6 < M_R < -15.7$. The photometric and kinematic properties of the brighter galaxies can be cast in terms of parameters which present little scatter with respect to a set of scaling relations known as the Fundamental Plane. To determine the form of these fundamental scaling relations at lower luminosities, we have measured velocity dispersions for a sample comprising 69 galaxies on the border of the dwarf and giant regime. Combining these data with our photometric survey, we find a tight correlation of luminosity and velocity dispersion, $L \propto \sigma^{2.0}$, substantially flatter than the Faber-Jackson relation characterising giant elliptical galaxies. In addition, the variation of mass-to-light ratio with velocity dispersion is quite weak in our dwarf sample: $M/L \propto \sigma^{0.2}$. Our overall results are consistent with theoretical models invoking large-scale mass removal and subsequent structural readjustment, e.g., as a result of galactic winds.

Key words: galaxies: clusters: individual: Coma; galaxies: elliptical and lenticular, cD; galaxies: dwarf; galaxies: kinematics and dynamics; galaxies: fundamental parameters; galaxies: evolution

1 INTRODUCTION

Dwarf galaxies ($M_R > -17.5$) are an important constituent of the Universe. They outnumber normal and giant galaxies, and form a distinct family of objects with very different fundamental properties from spirals and ellipticals (Kormendy 1985; Ferguson & Binggeli 1994). The form of the low-mass end of the galaxy mass distribution is an important diagnostic of galaxy formation theories (White & Frenk 1991). A clear understanding of the properties of dwarfs is essential to explore their relation to giant galaxies, to test galaxy formation models, and to establish a local calibrating sample to study properties of low-luminosity galaxies at high redshift. Since the dwarfs are likely to contain large amounts of dark matter in their haloes (Aaronson 1983; Mateo 1998; Wilkinson *et al.* 2002), any study of their evolution must also take account of their internal dynamics.

The fundamental plane (FP, Djorgovski & Davis 1987; Dressler *et al.* 1987) relating luminosity, velocity dispersion, surface brightness, and scale length for galaxies presents an important tool for the study of the dwarf galaxy population. In clusters more distant than Virgo and Fornax, spatially resolved spectroscopy becomes very

difficult, but it is still possible to measure integrated or central velocity dispersions of large samples with multi-object fibre fed spectrographs. Thus, it is now becoming feasible to examine how the kinematics of low surface brightness galaxies fit in with those of the better-studied giants.

There are serious questions over whether dwarfs follow a continuous sequence with brighter ellipticals in their photometric and kinematic parameters. Nieto *et al.* (1990) were among the first to extend the FP to galaxies with low luminosity and mass. From a sample of 17 galaxies with M_B in the range -19.4 to -15.3, they found that dwarf ellipticals form a low mass extension to the FP, with a scatter too large to be accounted for by measurement errors alone. They also found that the halo globular clusters lie on the faintward extension of the FP. Held *et al.* (1992, 1997) reached similar conclusions with a set of dwarf galaxies that excluded the two “most extreme” local group dwarf spheroidals, which are observed to have very high mass-to-light ratios. Incorporating galaxies with luminosities intermediate between the local group dwarfs and giant ellipticals, they found evidence for a continuous trend linking all the objects in their sample on the FP. Peterson & Caldwell (1993), on the other hand, assert that the fundamental plane for dwarf ellipticals is entirely different from that of the giants. Compiling a sample of strongly nucleated galaxies in the range $-17.8 < M_V < -16.1$ from the literature, they found a steeper dependence of luminosity on velocity dispersion and a change in mass-to-light ratio with luminosity. They claim that this supports scaling relations predicted by Dekel & Silk (1986, hereafter DS86) for the removal of interstellar gas by supernova driven winds in dwarf galaxies surrounded by dominant dark haloes. Nevertheless, their conclusions are heavily influenced by the inclusion of all the local group dwarf spheroidals; it remains to be seen whether these well represent the fundamental plane at faint magnitudes, and if the nucleation has substantially affected the results (cf. Geha, Guhathakurta & van der Marel 2002). Other studies have hypothesized that a mixture of formation mechanisms, including ram pressure stripping of gas-rich dwarf irregulars (van Zee, Skillman & Haynes 2004), primordial formation followed by gas loss in a supernova driven wind (DS86; Arimoto & Yoshii 1987; Yoshii & Arimoto 1987, hereafter YA87), “harassment” (Moore, Katz & Lake 1996), and tidal formation (Kroupa 1998), are involved in setting the observed galaxy properties.

More recently, Geha *et al.* (2002) and Geha, Guhathakurta & van der Marel (2003) have studied the FP for their sample of 17 Virgo dwarfs ($-17.52 < M_V < -15.48$), using the parameterisation of Bender, Burstein & Faber (1992). They showed that the dwarf ellipticals occupy a plane parallel to, but offset from, normal ellipticals. Graham & Guzmán (2003), however, have argued for a continuous progression of FP parameters based on detailed surface photometry from HST archival images for a sample of 18 dE galaxies in the Coma cluster. They modeled the surface brightness profiles with the more general Sérsic (1968) relation rather than the de Vaucouleurs (1948) law to uncover a strong correlation between the Sérsic index n , and absolute magnitude. In particular, they find that dwarfs have a Sérsic index in the range 1–2, and in all cases much less than the de Vaucouleurs law. They contend that application of the de Vaucouleurs law where it does not fit will result in derivation of incorrect surface brightness and size parameters, and that these differences will affect lower luminosity galaxies more. They conclude that the photometric scaling relations are continuous and linear, and hence normal and dwarf ellipticals form a single family. However, this does not explain why the dwarfs lie in a different region of the FP, as shown by Geha *et al.* (2003), who fit Sérsic profiles, and find indices in the range 1–2.

To extend the selection of data on intermediate-luminosity dwarf ellipticals and contribute to ongoing analysis of these objects, we are engaged in a major study of the properties of galaxies in the Coma cluster. From our deep photometric survey (Komiya *et al.* 2002, hereafter Kom02) we have constructed a spectroscopic sample (Mobasher *et al.* 2001, hereafter Mob01) with well defined selection functions. This has been used to investigate the dependence of their stellar components upon galaxy luminosity (Poggianti *et al.* 2001a), morphology (Poggianti *et al.* 2001b), and environment (Carter *et al.* 2002). Spectroscopic observations have been used to identify the cluster members and to investigate the dynamics within the clusters of the dwarf and giant populations (Edwards *et al.* 2002) and to study the properties of post-starburst galaxies and the correlation between their position and cluster substructure (Poggianti *et al.* 2004). Here we report on higher resolution spectroscopic observations of a subsample of these galaxies, in order to establish an unbiased FP. Studies of the faint extension of the FP, including ours, concentrate on galaxies in clusters. Largely this is for practical reasons: observations require long exposure times and to obtain sufficient samples multi-object spectrographs are required, which in turn require a high density of targets. While cluster galaxies are more affected by interactions with their environment than field galaxies, by studying regions of different density within the same cluster we can hope to quantify the effect of such interactions and to eliminate them as a source of uncertainty.

Two other recent studies address the same problem. The NOAO Fundamental Plane Survey (NFPS, Smith *et al.* 2004) is a large survey of over 4000 galaxies in 93 clusters. This survey concentrates on normal elliptical and lenticular galaxies, rather than the dwarfs. The survey was designed for clusters at a range of redshifts, and was carried out at a resolution approximately a factor three worse than ours; thus it is most reliable for velocity dispersions above 100 km s^{-1} . Matković & Guzmán (2005, hereafter MG05) and Matković & Guzmán (2007) present velocity dispersion measurements for a sample of faint early-type galaxies in the core of the Coma cluster. Again, their spectral resolution is worse than that of this study, by a factor of 1.6. Although they present velocity dispersions as low as 35 km s^{-1} , they require a correction for systematic errors at this dispersion, and our sample

is in general of galaxies of lower velocity dispersion. Furthermore, their sample is largely in the core of the cluster, whereas our sample contains both the core and lower density regions. Accordingly, our data put us in a position to provide a valuable extension to lower luminosity and less dense environment, with which to study the problem of the origin and properties of dwarf galaxies.

2 OBSERVATIONS

2.1 Source Selection

The spectroscopic targets for this study were selected from our wide-angle photometric (Kom02) and spectroscopic (Mob01), and subsequent papers in the series) catalogues of Coma cluster galaxies. The photometric catalogue provides B and R mags (to $R \sim 22$) and colours with an accuracy of 0.1 mag for three fields, covering 1.33 deg^2 in Coma. The spectroscopic catalogue covers the Coma1 (central) and Coma3 (~ 1 degree SW of the cluster centre, containing NGC 4839) fields, and was obtained using the Wide-field Fibre Optic Spectrograph (WYFFOS) on the William Herschel Telescope. The WYFFOS spectra, with a resolution of $6\text{--}9\text{\AA}$, yield redshifts (and hence cluster membership) and several spectral line indices sensitive to stellar population ages and metallicities (e.g. Poggianti *et al.* 2001a). The sample chosen for this present, higher-resolution spectroscopic study, was selected to include only spectroscopically confirmed members of the Coma cluster and to have $14.5 < R_{Kron} < 19.4$ and $19.5 < \langle \mu_R \rangle < 24.3 \text{ mag/arcsec}^2$, where R_{Kron} and $\langle \mu \rangle$ are the Kron magnitudes and average surface brightness over the Kron radius (an intensity weighted radius; Mob01), respectively. These limits correspond to $-20.6 < M_R < -15.7$, and thus our sample includes galaxies on either side of the boundary between dwarfs and giants, which we define following Mob01 to be at $M_R = -17.5$ or $R = 17.6$ at the distance of Coma, assuming a distance modulus of 35.1 for the cluster (Baum *et al.* 1997). For simplicity, we will primarily refer to these objects as dwarfs, given that the sample as a whole covers a distinct region of parameter space in luminosity and velocity dispersion compared to previous studies. Similar numbers of galaxies were observed in the high density core of the cluster, and in the outskirts (the Coma3 region of Kom02), with a total of 70 fibres on galaxies in the former and 65 in the later. The positional accuracy of the selected targets is $0''.5$, sufficient for spectroscopic purposes.

2.2 Spectroscopic Observations

The intermediate-resolution spectroscopic observations for the present study were obtained with the 3.5-m Wisconsin-Indiana-Yale-NOAO (WIYN) telescope, using the Hydra multifibre spectrograph. The targets were galaxies in the Coma1 and Coma3 fields, selected as described above. These fields were chosen to allow a large density contrast in the location of sample galaxies. The observations were performed over three nights between 28 April and 1 May 2003. We used an exposure time of 24×30 minutes and 14×30 minutes for Coma 1 and Coma 3 fields, respectively. The spectra covered a range $\sim 4700\text{--}5700\text{\AA}$ at $\Delta\lambda \sim 0.49\text{\AA}$ per pixel and 1.2 \AA spectral resolution, encompassing the region covered by Mgb and H β lines. Copper-argon lamp exposures were taken for wavelength calibration, and dome and twilight flatfields and bias frames were obtained. During each observation, approximately 80 out of the 100 $3''$ -diameter fibres were placed on target galaxies. The remaining fibres were assigned to sky. A number of standard stars with spectral types G8V–M0 III were also observed to provide velocity templates and calibration sources.

3 DATA REDUCTION

3.1 General procedures

Standard data reduction techniques were employed. All raw spectra were bias subtracted, using a collection of zero frames that were median-combined with a cosmic-ray rejection algorithm. Sets of dome and twilight flatfield images taken at the beginning and end of each night were combined in a similar manner. Arc lamp exposures taken in succession were also combined. Subsequent data reduction was performed with the IRAF DOHYDRA package. Spectra were flatfielded, sky subtracted, wavelength calibrated, scattered light subtracted, cleaned of bad pixels, and corrected for varying fibre throughput (using flatfields). One night sky line, at 5577 \AA , partially remained and was masked out of later spectral analysis. After object spectra were extracted, all frames taken of each field were combined using median scaling and cosmic ray rejection. Sky subtraction was neglected for the short exposures of bright standard stars. The final spectra were rebinned to a log-linear wavelength scale with 2048 pixels. Signal-to-noise values were substantially lower than expected (i.e., 60% of the targets had signal-to-noise ratios of 10 per \AA or lower), but none the less our spectral resolution still allows us to derive velocities with reasonable uncertainties, as discussed in §3.3. Several example spectra are shown in Figure 1.

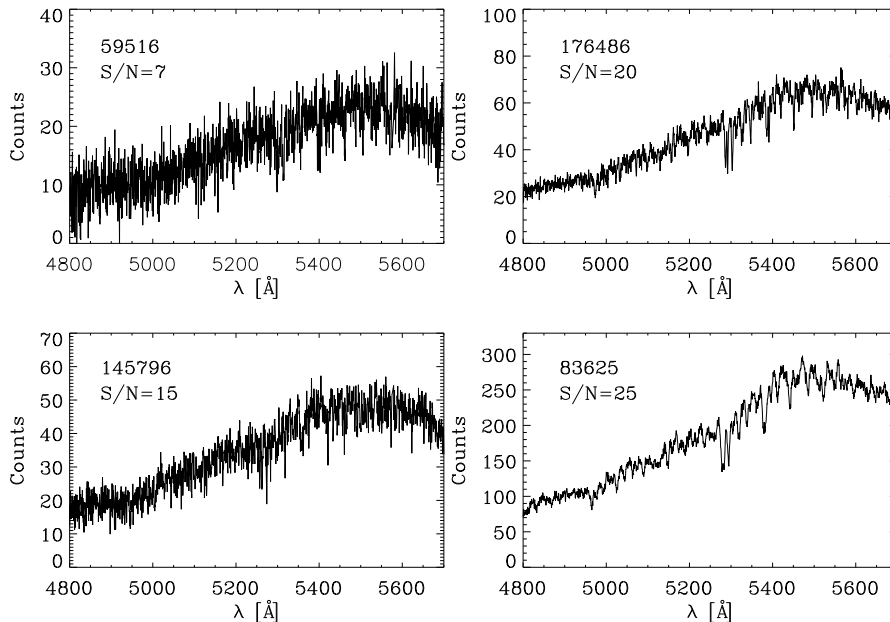


Figure 1. Examples of spectra with various signal-to-noise values. The Komiyama identification number is shown (see Table A1).

3.2 Radial velocities and dispersions

To measure the redshift and amount of broadening present in each galaxy spectrum, we adopted the Fourier cross-correlation technique, originally developed by Tonry & Davis (1979). We chose this over more sophisticated methods that provide second-order velocity moments, because of the limitations of our mediocre signal-to-noise levels. Galaxies were cross-correlated with each of five stellar velocity templates, using the IRAF package FXCOR. All spectra were apodised down to 5% at the ends with a cosine bell. In addition, they were filtered in the Fourier domain with a ramp function to remove additional unwanted noise.

Galaxy spectra were cross-correlated with the template spectra in the region 4740 to 5726 Å, with the night sky line masked out. Four template stars—HD 62509, HD 65583, HD 75839, and HD 90861—were observed with the same spectroscopic setup and comprised spectral types G8V, K2 III, and K0 IIIb. HD 65583 was observed with two different fibres. Redshifts were computed from the position of cross-correlation peaks, and velocity dispersions were determined from the widths of the peaks. In order to convert from full-width at half maximum (FWHM) of the cross-correlation peaks to a true velocity dispersion, calibration curves were produced by broadening the template stars with gaussian kernels of different velocities, and cross-correlating the resulting spectra against the original templates. This technique allows for reasonably accurate measurement of dispersions down to the instrumental resolution limit where the FWHM reaches $\sim 120 \text{ km s}^{-1}$. At the distance of the Coma Cluster ($\sim 105 \text{ Mpc}$), the $3''$ diameter aperture is equivalent to 1.53 kpc. Hence our velocity dispersions are effectively averaged out to a radius of 0.76 kpc. We believe this is preferable to obtaining central velocity dispersions, since Geha *et al.* (2002) have shown that galactic nuclei occupy a region of the fundamental plane separate from the underlying galaxy, and much closer to the globular clusters (a low-mass, high surface brightness region). To assess the degree of mismatch between template spectra and galaxies, we examined the spread of dispersion values obtained for each galaxy. No individual template produced consistently discrepant dispersions, and the $1\text{-}\sigma$ variation of values returned by different templates was typically $1\text{--}5 \text{ km s}^{-1}$. Although the spread in the spectral types is small enough that perhaps little velocity variation would be expected, tests using more extensive template sets (see §4.1) did not produce systematic shifts in the results. Hence, for each galaxy we averaged the results of all templates. We used the Tonry-Davis R coefficient (TDR; Tonry & Davis, 1979) as a measure of goodness of fit to the cross-correlation peak; typically TDR values less than 3.0 are unreliable. However, our adopted signal-to-noise requirement of $S/N > 7$ (§3.3) proved to be the dominant selection criterion, leading to the removal of all but one galaxy (GMP 4351) with $TDR < 6$ from the sample. This remaining galaxy was retained since no single cross-correlation template produced a TDR value less than 3.0.

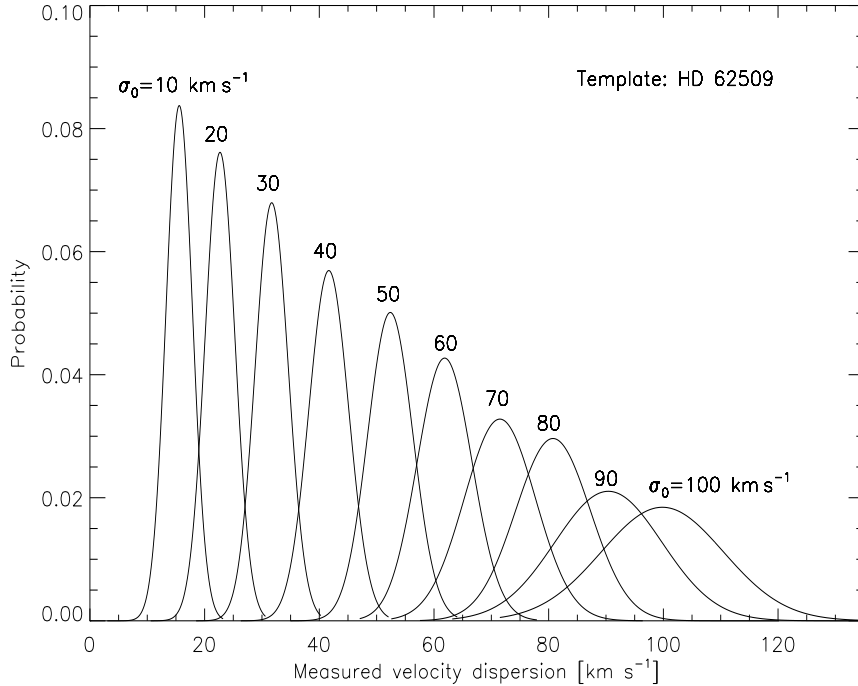


Figure 2. Results of cross-correlating the spectrum of template star HD 62509 with fake galaxies of $S/N=15$ per \AA and velocity dispersions from $\sigma_0=10$ to 100 km s^{-1} . Each distribution of measured velocity dispersions shown is derived from a run of 300 simulations in which the template spectrum was cross-correlated against a fake galaxy with a particular broadening σ_0 (as noted above each plotted distribution) and a gaussian was fit to the results.

3.3 Error analysis

The primary source of uncertainty in our results is poor signal-to-noise. We suspect that misalignments of the fibres with the target galaxies due to a combination of astrometric measurement and transformation and physical positioning errors is responsible for this problem. To determine the relationship between signal-to-noise and accuracy of dispersion measurements, we have performed bootstrap simulations in which template star spectra are broadened to a variety of velocities, combined in equal proportions of spectral types to create a “fake” galaxy, and subsequently augmented with random noise to achieve a particular signal-to-noise ratio (S/N). The resulting “galaxy” spectrum is then cross-correlated with the original templates to determine what the range of measured velocity dispersions would be. The process of adding noise and measuring the dispersion is carried out 300 times for each S/N and velocity broadening value, and a gaussian is fit to the results. An example simulation for the template star HD 62509 cross-correlated against fake galaxies with $S/N=15$ per \AA and broadening values, σ_0 , from 10 to 100 km s^{-1} is shown in Figure 2. Although each value of σ_0 leads to a symmetric, gaussian distribution of measured dispersion, in some cases there are offsets between the value of σ_0 and the mean measurement. This occurs particularly at low dispersions where the cross correlation method tends to produce overestimates. As explained below, we include this effect as an additional source of uncertainty. At higher dispersion, the larger broadening values also lead to a larger spread. Nevertheless, the widths and peaks of the distributions follow regular trends across the entire range of σ_0 , to which we have fit polynomial functions; this enables us to predict the distribution resulting from any σ_0 .

Calculating the uncertainties for a *measured* dispersion σ_m requires an inversion of these distributions to obtain the probability that it was derived from any *true* dispersion, σ_0 (what is plotted in Figure 2 shows the opposite). We have done this by discretising the probability distribution in increments of 1 km s^{-1} up to a maximum of 140 km s^{-1} : for each $\sigma_{0,i} \in \{1, 2, 3, \dots, 139, 140 \text{ km s}^{-1}\}$, the probability of measuring σ_m is denoted $P(\sigma_m|\sigma_{0,i})$. We solve for the values of $P(\sigma_m|\sigma_{0,i})$ by integrating the gaussian distributions for each $\sigma_{0,i}$ from $\sigma_m-0.5 \text{ km s}^{-1}$ to $\sigma_m+0.5 \text{ km s}^{-1}$, since our measurements are probably not accurate to better than 1 km s^{-1} . The conditional probability for true dispersion is hence given by:

$$P(\sigma_{0,k}|\sigma_m) = P(\sigma_m|\sigma_{0,k}) / \sum_{i=1}^{140} P(\sigma_m|\sigma_{0,i}).$$

The results of this computation are displayed in Figure 3.

The resulting distributions of velocity dispersion illustrate how accurate our measurements are for low S/N .

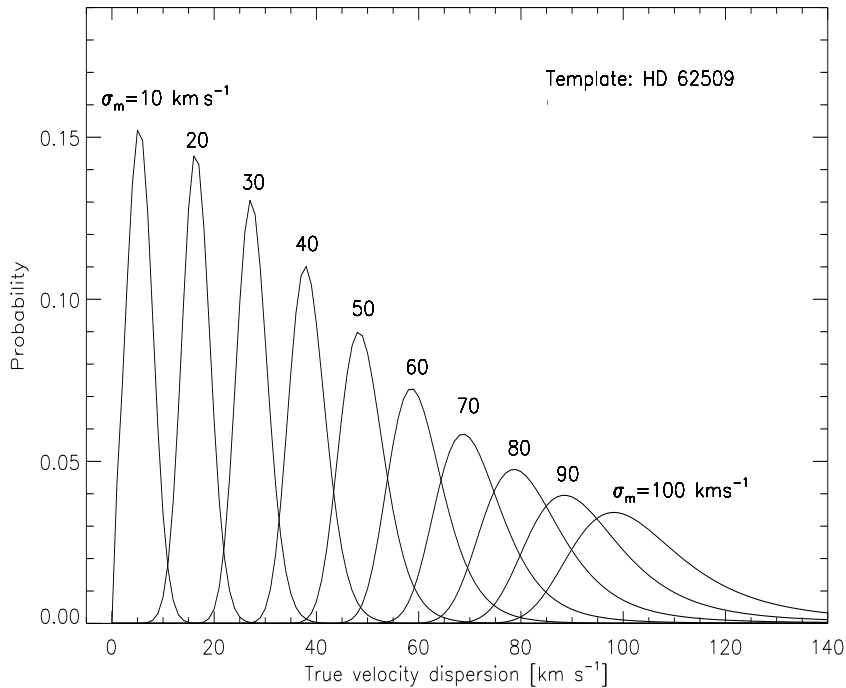


Figure 3. The distributions in Figure 2, inverted to give the probability of true velocity dispersion as a function of the measured value (where the measured values, σ_m , are plotted in increments of 10 here).

As seen in Figure 3, they are slightly asymmetric, due to the fact that larger velocity dispersions produce a larger spread in the measured σ . Velocity dispersion is also correlated with galaxy brightness, in the sense that giant ellipticals have both larger velocity dispersions and luminosities than dwarfs. Therefore, because we observed the galaxies in the sample for equal periods of time, low dispersion values correlate with low S/N.

For each value of S/N, we combine the results of simulations involving each of the five template stars. The 1- σ uncertainties for each velocity dispersion value are derived by integrating the distributions in Figure 3 to $\pm 34.1\%$ of their total area to either side of the peak. If the peak does not fall on the measured value, the difference between these two is incorporated (added in quadrature) as a systematic error. After adding the 1- σ uncertainties from each template in quadrature, we find that we can measure dispersions near 15 km s^{-1} with 25% accuracy at $S/N \lesssim 7$ per \AA and near 25 km s^{-1} with 15% accuracy for $S/N \sim 8$. We attain 6% accuracy for the galaxies that have $\sigma \sim 35 \text{ km s}^{-1}$ and $S/N \sim 15$. For S/N values above 20, and dispersions larger than 40 km s^{-1} , we achieve an uncertainty of 3%. Because accurate dispersion measurements require reasonably high signal-to-noise ratios, we have disregarded most spectra with $S/N < 7$. This condition was relaxed for several of the dwarfs with very low velocity dispersion; errors of $\sim 25\%$ were permitted for these objects, since we believe it is important to extend the sample to galaxies with low surface brightness.

Uncertainties were calculated individually for each of the galaxies and are quite small—on the order of 2–4 km s^{-1} . The derived uncertainties could be overly optimistic—especially given that our fake galaxy spectra consist of only five stars (of which one is the exact template), as opposed to millions in a true galaxy spectrum. We discuss this further in § 4.1. However, our confidence is increased by the fact that in most cases, the spread in velocity dispersion measurements from the five different template spectra is *less* than the uncertainty we have estimated from the simulations. The final tally of galaxies observed that we believe to have reliable velocity dispersion measurements includes 36 galaxies in Coma 1 and 33 galaxies in Coma 3.

4 RESULTS

We present our measured velocities and velocity dispersions in Table A1. In this table column 1 gives the identification from Godwin, Metcalfe & Peach (1983); column 2 the identification from our own programme (Kom02, Mob01); column 3 a morphological type, estimated visually from the R band mosaic CCD image; columns 4 and 5 the J2000 position of the galaxy; columns 6 and 7 the R-band and B-R Kron magnitude (see Kom02 for a definition); column 8 the effective R-band surface brightness (average surface brightness within the effective radius; Kom02), columns 9 and 10 the heliocentric recession velocity and its error in km s^{-1} ; columns 11 and 12

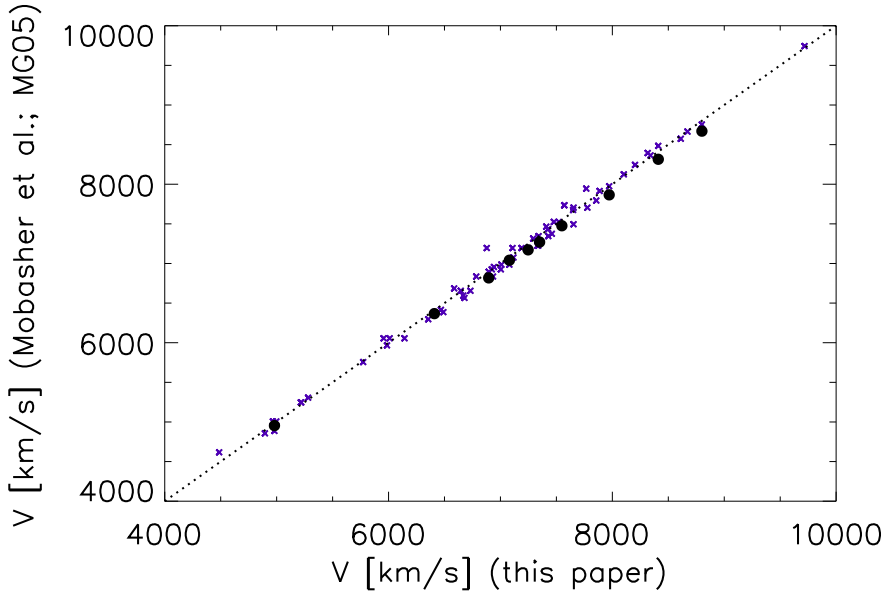


Figure 4. Velocity from Mob01 (crosses) and from MG05 (filled circles) plotted against velocity from this paper. The straight line shows equality, indicating that the MG05 values are systematically lower.

the velocity dispersion and its error in km s^{-1} ; and column 13 the signal-to-noise per \AA . In column 3, E and dE galaxies are delineated by the boundary $M_R = -17.5$ ($R = 17.6$ at the distance of Coma) chosen by Mob01.

4.1 Comparison with external data

We compare our radial velocities with those derived from our WYFFOS observations of a larger spectroscopic sample (Mob01). All of our galaxies already have velocities from that paper, and in Figure 4 we compare the velocities. The mean difference between the two datasets is 2.7 km s^{-1} , in the sense that the WYFFOS velocities are higher, and the scatter about the linear relation is 81 km s^{-1} . Most of the scatter can be attributed to errors on the WYFFOS velocities, which were obtained at lower resolution. Ten of our galaxies are common with the sample of MG05. These velocities are also compared in Figure 4. The mean difference in this case is 75 km s^{-1} , in the sense that our velocities are higher, with a scatter of 32 km s^{-1} . We conclude that there is a systematic offset in the velocity system of the MG05 data, of about 75 km s^{-1} , but that the random error in each dataset is of the order $32/\sqrt{2} \sim 22 \text{ km s}^{-1}$. The random error in our WYFFOS dataset is probably twice this.

In Figure 5 we compare the velocity dispersions with those of MG05 for the ten galaxies in common. There is considerable scatter about the 45 degree line in this plot; however this plot only covers a small range in $\log \sigma$. We find that a formal fit gives an offset in $\log \sigma$ of 0.157, in the sense that MG05 dispersions are higher, and an rms of 0.171 about this value. However a substantial part of this is due to a single galaxy, GMP3018, for which we measure a dispersion of 20 km/s , and MG05 measure 75 km/s . The cause of this is unclear, it could be due to a misidentification in one of the two studies, or it could be due to poor signal-to-noise (of the ten galaxies in common, GMP has the lowest signal-to-noise in both studies).

At the suggestion of the referee, we have investigated whether the offset is systematic, as might be caused by a calibration error in one study or the other, or is due to a signal-to-noise problem. In Figure 6 we plot the differences in $\log \sigma$ against S/N from each study. The most likely cause of the differences would appear to be effects due to the poor signal-to-noise in the fainter galaxies. Given that our spectral resolution is a factor two higher than MG05, and given also that the strongest correlation is with their S/N, it is likely that our dispersions are reliable to lower values. However, even with our resolution, dispersions below 30 km s^{-1} are likely to be systematically too high.

In figure 6 we show also linear least-squares fits as a function of signal-to-noise. The linear fits are:

$$\Delta(\log \sigma) = -0.32(\pm 0.13) + 0.013(\pm 0.008) * S/N(\text{this study})$$

$$\Delta(\log \sigma) = -0.37(\pm 0.09) + 0.012(\pm 0.004) * S/N(\text{MG05})$$

In section 4.2 we will use the second of these two relations to transform the MG05 dispersions onto our system.

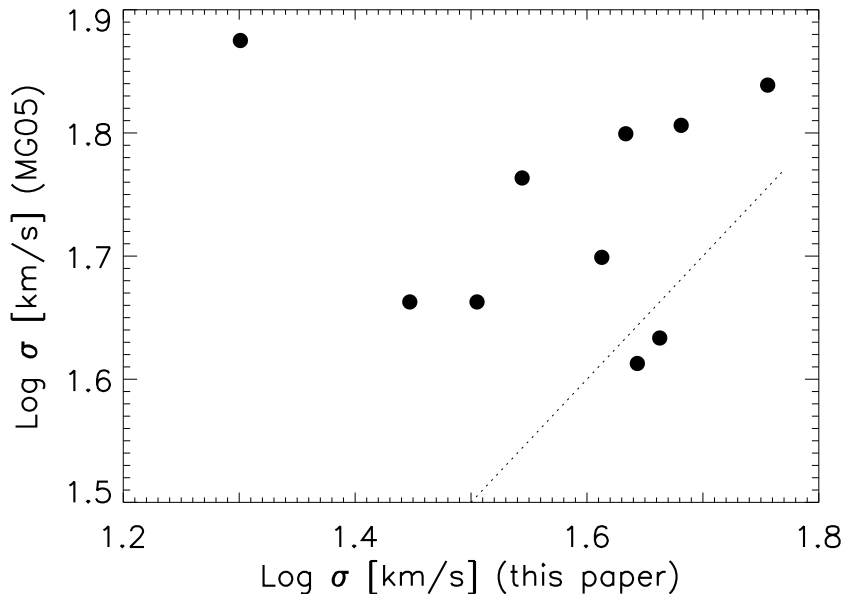


Figure 5. Velocity dispersions from MG05 plotted against those from this paper. The straight line shows the locus of equal velocities; MG05 velocity dispersions are systematically higher.

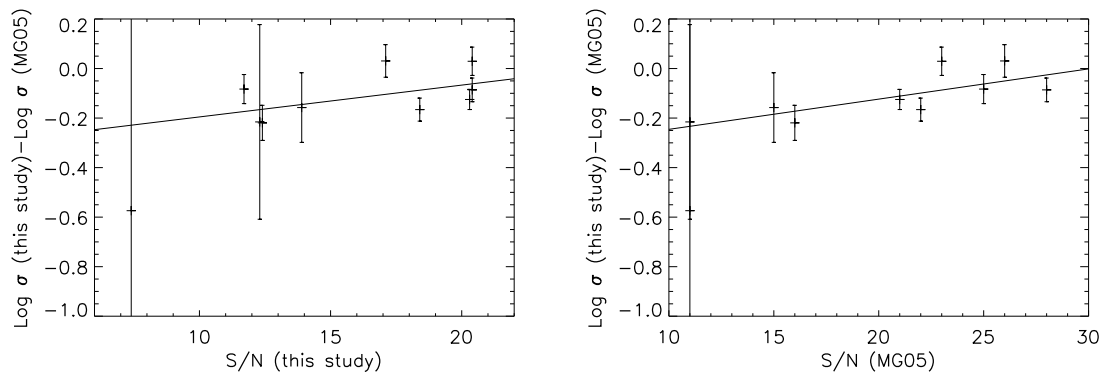


Figure 6. Offset in $\log \sigma$ between our study and MG05, plotted against the signal to noise in our study (left panel) and in MG05 (right panel). The correlation coefficients are 0.52 and 0.74 respectively. The fits shown and discussed in the text omit the most discrepant galaxy, GMP3018.

We estimate that this fit only applies for S/N values up to 30, above which there is sufficient agreement between the two datasets. Due to the large measurement uncertainties, we do not fit higher order functions to the data.

To ensure that our lower dispersion measurements are not strictly the result of the method of computing velocity dispersions, we have performed an additional analysis with the Penalized Pixel-fitting method (pPXF; Cappellari & Emsellem 2004). This approach reconstructs the line-of-sight velocity distribution via a parametric fit to the galaxy spectra using large numbers of stellar templates. For high signal-to-noise data, it permits the extraction of higher order moments of the velocity distribution. However, for the lower S/N values of our spectra, we do not expect to accurately measure departures from a gaussian profile. Hence, we employ pPXF as a check on the dispersions for the subset of ten galaxies in common between our data and those of MG05, but retain FXCOR as our method of choice for the overall results.

For each galaxy in the comparison, we have computed velocity dispersions with both FXCOR and pPXF using several different sets of stellar template spectra. In addition to the five templates obtained with our Hydra setup, we have incorporated large numbers of spectra from the Indo-U.S. Library of Coudé Feed Stellar Spectra (Valdes *et al.* 2004). The pPXF program efficiently computes velocity dispersions for large sets of templates, thereby allowing us to eliminate the effects of template mismatch. Among the template sets used to measure dispersions were five Coudé Feed Library (CF) templates with spectral types matched to those of our Hydra

spectra, 60 CF templates with spectral types ranging from A through M, 40 CF templates with spectral types from G to M, and two CF spectra for stars in our Hydra sample (HD 62509 and HD 65583). To compare the different realizations of dispersions, we have degraded the CF spectra to the resolution of Hydra and computed the average offset between measurements of the same galaxies. To determine the significance of these differences, we apply the Kolmogorov-Smirnov (KS) test to different pairs of dispersion measurements on all ten galaxies. Our results indicate that FXCOR and pPXF return galaxy velocity dispersions that agree to within 5% ($< 2 \text{ km s}^{-1}$ offset, of the order the uncertainties), or a significance of 98% when the same template set is used. This confirms that the measurements are not dependent on the computational method. We also find that regardless of templates or method used, dispersions measured for our ten galaxies in common with MG05 are systematically offset by $\sim 40\%$, at a significance of 90–95% (i.e., only a 5–10% chance that these differences are due to random variation). We conclude that the difference between our measurements and those of MG05 is real, at least at the low dispersions of the 10 galaxies in question.

In addition, we have used the results of our tests with pPXF to assess the dependence of the velocity dispersions on the number of templates and their spectral types. The majority of these experiments produced results in agreement with our original measurements using FXCOR and Hydra templates. However, in a few cases the agreement is only marginal (67% level). Surprisingly, the most discrepant velocity dispersions resulted from a trial of five CF templates with spectral types matching those of the five Hydra templates. The two sets of templates produced dispersions differing by an average of 5 km/s, a disagreement at the 31% level). This cannot be due to template mismatch, and we attribute the disparity to differences in instrumental setup and resolution (despite the fact that we have degraded the CF spectra to match ours). We also note that in the cases where CF library templates yield significantly different velocity dispersions from those of the Hydra templates, the measurements are always *lower*. Hence, this does not explain the even larger discrepancy with the MG05 results. Because there appears to be an unknown source of $\sim 3 \text{ km s}^{-1}$ variation in the results that is not accounted for by template mismatch, we incorporate it as an additional uncertainty to our velocity dispersions. Errors listed in Table A1 are thus the formal uncertainties calculated in §3.3, plus a template mismatch error given by the average difference between dispersions from different Hydra templates, plus the 3 km s^{-1} additional uncertainty, all added in quadrature.

4.2 Trends with velocity dispersion

To assess our data in the context of the well-known properties of giant ellipticals, we have plotted a number of photometric parameters for galaxies from Mob01 against the velocity dispersions. The velocity dispersion values for our galaxies are almost exclusively less than 100 km s^{-1} , while the vast majority of those measured for galaxies traditionally considered “giants” are greater than 100 km s^{-1} , and often 200 km s^{-1} . In Figure 7 we plot the relation between $\log \sigma$ and absolute magnitude in the R band. The distribution of parameters can be seen in the accompanying histograms. The absolute magnitudes in this fit were derived from our R band apparent magnitude within three Kron radii (Mob01), again assuming a distance modulus of 35.1 magnitudes, and an extinction in the R band of 0.03 magnitudes (Bernstein *et al.* 1995). Different symbols in this plot represent different morphological types (from Table A1).

Our sample contains four galaxies which according to our visual classification are, or might possibly be, spirals (crosses in Figure 7). In calculating our best-fitting regression line, we exclude these galaxies, and find a relation $\log \sigma = -2.1 \pm 0.4 - (0.20 \pm 0.02)M_R$. In this and all other regression fits we minimise residuals in $\log \sigma$, as the errors in this quantity are far larger than those on the photometric parameters. This gives an $L - \sigma$ relation of the form $L_R \propto \sigma^{2.0 \pm 0.2}$, which is substantially flatter than the Faber-Jackson relation for giant ellipticals ($L \propto \sigma^4$, Faber & Jackson 1976) but consistent with results presented by MG05 and previous authors.

To investigate whether the inclusion of galaxies with low signal-to-noise spectra might bias the results, we have repeated the analysis, excluding those galaxies with spectra with $S/N < 10$. In figure 8 we plot the remaining galaxies, and the fit to the slope of the $L - \sigma$ relation. We find $\log \sigma = -1.2 \pm 0.4 - (0.16 \pm 0.04)M_R$, giving $L_R \propto \sigma^{2.5 \pm 0.8}$, so the slope does not differ significantly from that for the whole sample.

To increase the size of our sample at the brighter end of this correlation, for those galaxies in common between MG05 and Mob01 we have moved the MG05 dispersions onto our system, using the second of the two linear correlations presented in Section 4.1. In figure 9 we plot our dispersions and the transformed MG05 values, together with a fit showing an $L - \sigma$ relation of the form $L_R \propto \sigma^{1.84 \pm 0.10}$, entirely consistent with that defined by our sample alone.

In Figure 10 we plot $\log \sigma$ against the effective surface brightness from Mob01. The best-fitting linear regression line is $\log \sigma = 6.7 \pm 0.5 - (0.25 \pm 0.02)\mu_{\text{eff}}$, where μ_{eff} is the average R band surface brightness within the effective radius, in magnitudes arcsec^{-2} . This corresponds to a relation of the form $I_m \propto \sigma^{1.6 \pm 0.2}$, where I_m is effective surface brightness in flux units, in the R band. The relationship between surface brightness and velocity dispersion also differs from that of the giant ellipticals. Using the result of $L \propto I_m^{-1.5}$ from Binggeli, Sandage &

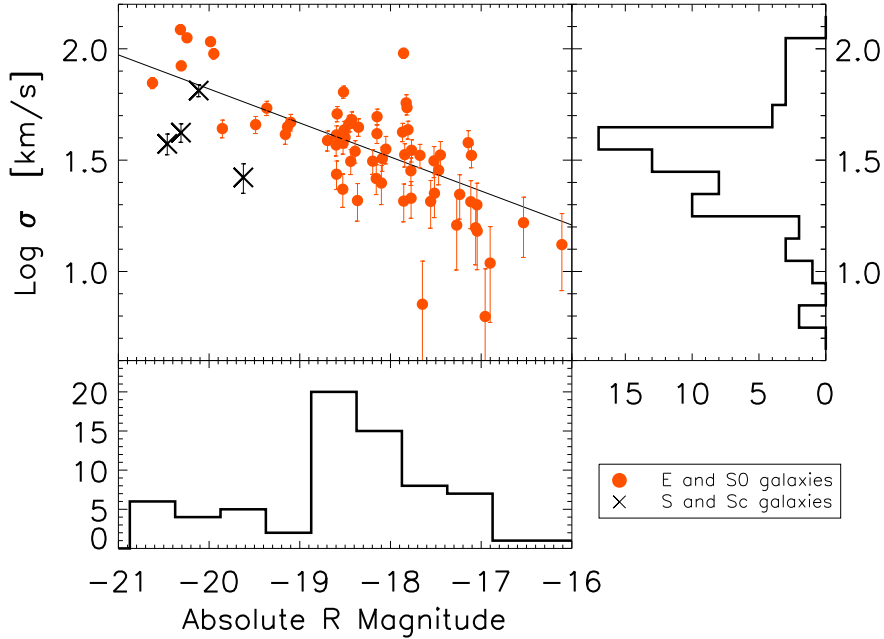


Figure 7. Relation between $\log \sigma$ and absolute magnitude for our sample. In this plot, the different symbols represent different morphological classifications: filled circles are ellipticals or S0 galaxies, and crosses are galaxies classified as spirals or possible spirals. The fit shown by the straight line is given by $\log \sigma = -2.1 \pm 0.4 - (0.20 \pm 0.02) M_R$, and the points representing spirals have been excluded.

Tarengi (1984) with the Faber Jackson relation, we expect $I_m \propto \sigma^{-2.5}$ for giant elliptical galaxies. Our value for the lower-luminosity galaxies in this sample is thus quite different.

Another trend to explore is that of velocity dispersion and effective radius. The latter is directly related to luminosity and effective surface brightness via $L = 2\pi I R_e^2$. Using our measured relationships between σ , luminosity and surface brightness we derive $R_e \propto \sigma^{0.19 \pm 0.14}$. This is just consistent with the relation that would be derived using the established $L - R_e$ trend for dwarf ellipticals (Binggeli *et al.* 1984), which is $L \propto R_e^4$ and the measured $L - \sigma$ relation from MG05 and our work, which would together give $R_e \propto \sigma^{0.5}$. It is however inconsistent with the relation for giants, derived from Fish’s (1964) law ($L \propto R_e^{1.2}$) and the Faber-Jackson relation, which together imply $R_e \propto \sigma^{3.3}$.

Since the mass-to-light ratio, M/L , is an important indicator of galaxy properties, we have computed its variation with σ for our dwarf sample. Assuming the galaxies we have observed form a homologous sequence, we can compute the expected M/L as a function of σ by applying the virial theorem (e.g., Mobasher *et al.* 1999; D’Onofrio *et al.* 2006). This results in $M/L \propto \frac{\sigma^2}{I_m R}$ (e.g. Richstone & Tremaine 1986). Regarding the radius as an independent parameter, we express it in terms of surface brightness and luminosity to obtain $M/L \propto \frac{\sigma^2}{\sqrt{I_m L}}$. Substituting our observed dependence of L and I_m upon σ , we obtain $M/L \propto \sigma^{0.19 \pm 0.14}$.

4.2.1 Trends with Radius within the cluster

The mechanisms proposed to explain the differences in scaling laws between giants and dwarfs (Section 1) may be affected by environment. In particular, winds may be constrained and ram-pressure stripping enhanced by the hot gas density in cluster cores, and the importance of harassment and tidal dwarf formation depends upon both the galaxy density and velocity dispersion. Furthermore, Smith *et al.* (2008), working in precisely the same regions of the Coma cluster, found a significant environmental dependence of the stellar population properties in dwarf galaxies, and thus evidence of environmental influence on the star formation history. As our sample includes galaxies in the infall region of the cluster, we can search for a possible environmental dependence of the $L - \sigma$ relation, as a counterpart to the environmental dependence of the properties of the stellar populations. To undertake this comparison we divide our sample into the Coma1 and Coma3 regions of Kom02, which separates the sample at a clustocentric radius of 0.49 degrees. However, our sample has a different luminosity distribution within these two regions; the outer Coma3 sample contains many more galaxies with $M_R < -19$, so we limit this analysis to galaxies with $M_R > -19$.

In Figure 11 we show the $L - \sigma$ relation for our inner and outer fields. The slope of the fit is shallower in the

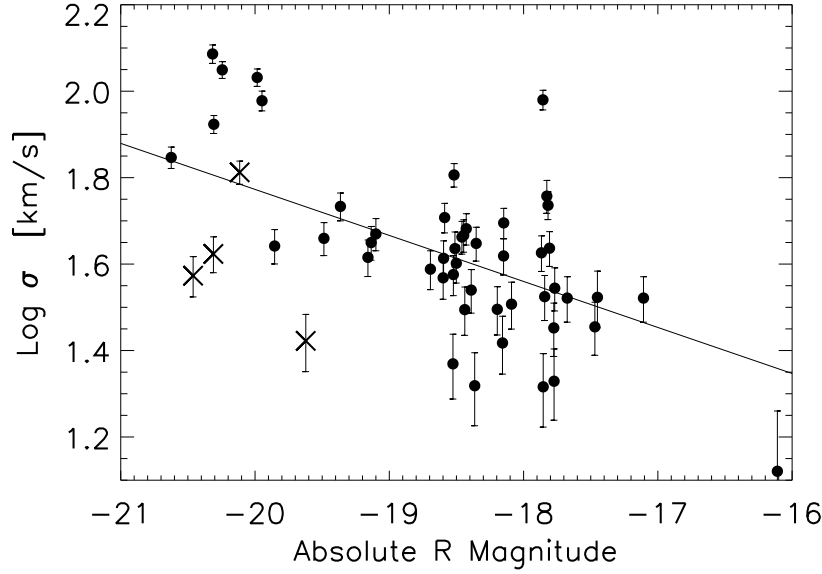


Figure 8. Relation between $\log \sigma$ and absolute magnitude for the E and S0 galaxies with $S/N > 10$. Symbols are the same as in Fig. 7. The fit to the high S/N galaxies is given by $\log \sigma = -1.2 \pm 0.4 - (0.16 \pm 0.04)M_R$.

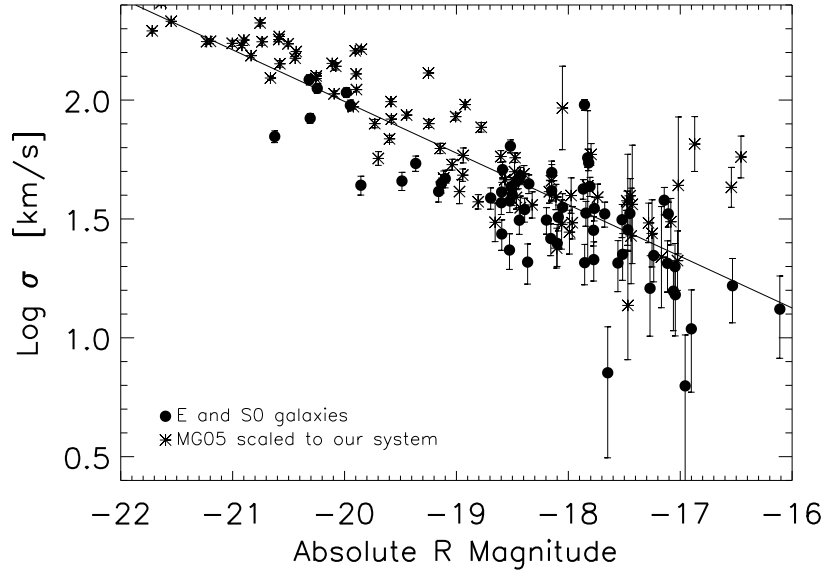


Figure 9. Relation between $\log \sigma$ and absolute magnitude for the E and S0 galaxies in our sample and for the sample of MG05, adjusted to our velocity dispersion system as described in the text (asterisks). The fit shown by the straight line is to both samples, with galaxies in both samples included twice, and is given by $\log \sigma = -2.35 \pm 0.21 - (0.217 \pm 0.011)M_R$.

outer field ($L_R \propto \sigma^{1.29 \pm 0.29}$ as opposed to $L_R \propto \sigma^{2.21 \pm 0.40}$). Despite the marginal significance of the difference we find, this possible environmental effect merits further investigation by increasing the sample, and thus lowering the error bar, in the outer region.

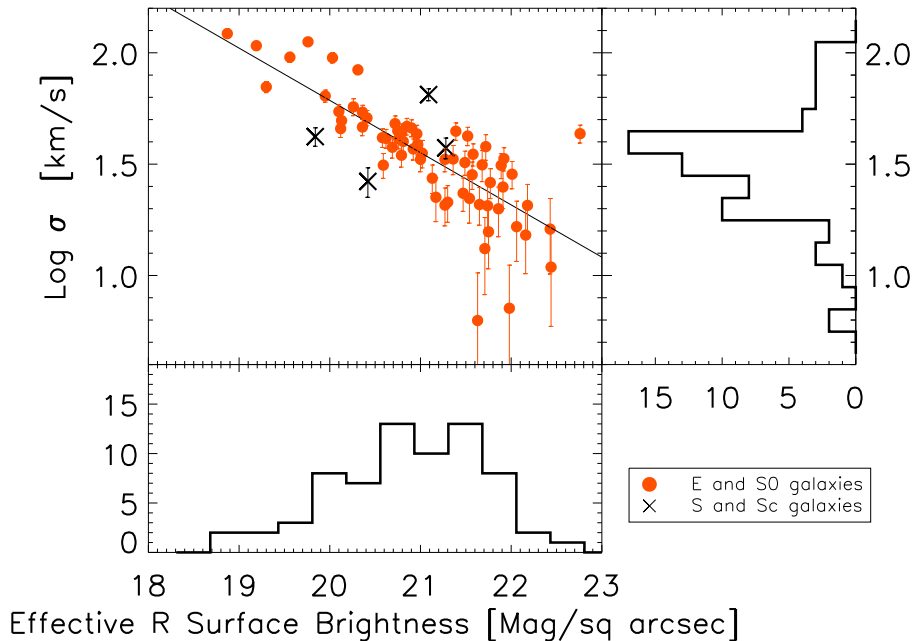


Figure 10. Log σ against effective R band surface brightness. The symbols have the same meaning as in Figure 7. The trend is given by $\log \sigma = 6.7 \pm 0.5 - (0.25 \pm 0.02) \mu_{\text{eff}}$. Again, the fit has been calculated omitting the spirals.

5 DISCUSSION

Our results confirm that galaxies in the dwarf regime do not follow the standard empirical relations established for giant ellipticals. Of primary interest is the fact that the $L - \sigma$ relation for dwarfs is substantially shallower than the classical Faber-Jackson relation. This was initially suggested by Davies *et al.* (1983), whose kinematic study of 11 faint elliptical galaxies with $M_R > -20.8$ led to $L \propto \sigma^{2.4 \pm 0.9}$. Many independent studies have found a relation between $L \propto \sigma^{2.0}$ and $L \propto \sigma^{2.55}$ in the R or B band (Held *et al.* 1992; De Rijcke *et al.* 2005; MG05). Peterson & Caldwell (1993), on the other hand, found a much steeper $L_V \propto \sigma^{5.6}$ by including the local group dwarf spheroidal galaxies. Our study indicates that in an intermediate luminosity range, $-19 < M_R < -16$, galaxies continue to follow the shallower relation. In addition, the observed relation between surface brightness and velocity dispersion is different from that of giant ellipticals but consistent with that implied by the position of dEs in Figure 1c of De Rijcke *et al.* (2005).

To confirm that the derived scalings for dwarf galaxies are substantially different from those of the giants, we must assess potential sources of bias. Surface brightness selection and morphological misclassification of low surface brightness galaxies can bias the sample—although elliptical and lenticular galaxies follow the same $L - \sigma$ relations (Jørgensen & Franx 1994), spiral galaxies do not. Performing a linear regression on *all* of the data plotted in Figure 7, we find that the effect of contamination by spirals on the $L - \sigma$ relation is to increase the index; thus inclusion of late-type galaxies does not explain the difference from the Faber-Jackson relation for giants. Likewise, the difficulty in measuring velocity dispersion for the low surface brightness galaxies could produce erroneously high σ values, but would also have the effect of raising the index in the $L - \sigma$ relation. The same reasoning holds for the run of surface brightness versus velocity dispersion; the index of the $I_m - \sigma$ relation would increase due to spiral contamination, and the implied $L - R_e$ relation would only change slightly.

Finally, we address the possibility that the luminosity and velocity dispersion values are systematically affected by the way we have defined these parameters. Luminosities have been derived from Kron magnitudes, which have been shown to agree with standard fixed-aperture magnitudes to within 2% (Mob01). If this is a cause of measurement bias, such a percent-level effect would be well within the scatter of the data. Velocity dispersions must also be carefully defined, as some studies report central values, while others provide averages over a particular galactic radius. Fortunately, radius-dependent studies of velocity dispersion have shown that it varies only on the order of 10% out to large radii (e.g., Bender & Nieto 1990). Our own velocity dispersions have been measured over a $3''$ diameter, equivalent to 1.53 kpc. As discussed in § 3.2, we believe this is preferable to obtaining a truly central measurement, to sample kinematics that are not dominated by the nucleus. In addition, a number of studies on giants to which we compare our data have also used normalized apertures, as suggested by Jørgensen, Franx, & Kjørgaard (1996). With this approach, Jørgensen (1999) obtained velocity dispersions for Coma giants within a $3.4''$ diameter, corresponding to 1.73 kpc. The similar aperture size employed in the present study allows

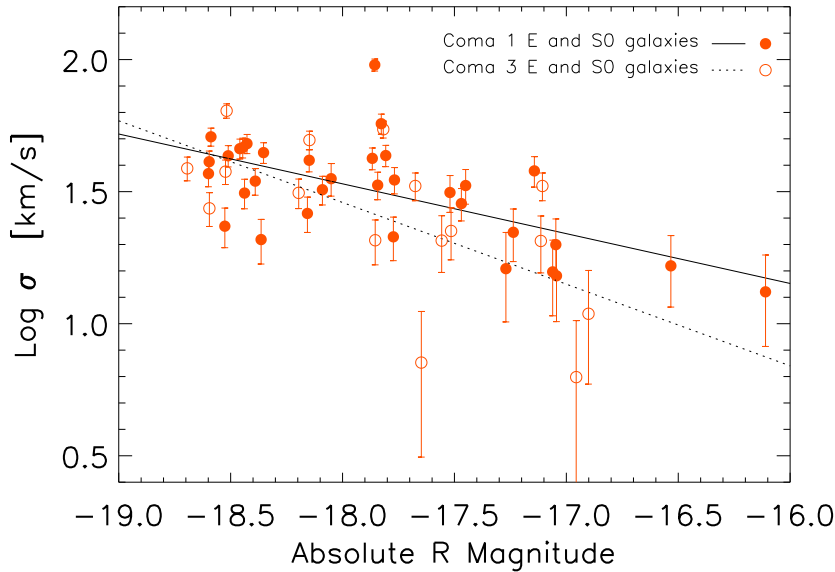


Figure 11. Relation between $\log \sigma$ and absolute magnitude for the E and S0 galaxies with $M_R > -19$ in the Coma1 field inside 0.49 degrees radius (filled circles), and in the Coma3 field outside 0.49 degrees radius (open circles). The solid line shows the fit to the inner field, and is $\log \sigma = -1.87 \pm 0.73 - (0.19 \pm 0.04)M_R$, while the dashed line is the fit to the outer field, $\log \sigma = -4.11 \pm 1.80 - (0.31 \pm 0.10)M_R$.

for a direct comparison with these data. Thus we are confident that the differences between the relations shown in Figures 7 and 10, and the equivalent relations for brighter galaxies, reflect the intrinsic properties of the samples, and are not due to biases in the sample selection or the methods employed to make the measurements.

It is unclear whether there is a true dichotomy between giants and dwarfs, or simply a continuous set of relations with gradually changing slopes. Nevertheless, we can explore the possible reasons for the observed dwarf galaxy scalings by comparing them with theoretical predictions based on the physical processes thought to operate in these galaxies. Although rotation was initially suggested as a cause for the differing kinematic parameters, and specifically the flattening of dwarf galaxies, recent work by Simien & Prugniel (2002), Geha *et al.* (2003), and MG05 has cast doubt on this idea. The anisotropic velocity dispersions observed in dwarfs have been also accounted for by invoking galactic winds spawned by supernovae, as suggested by Bender & Nieto (1990). Winds are thought to dominate in objects with velocity dispersions under 60 km s^{-1} (Schaeffer & Silk 1988). The processes of gas loss, galaxy inflation and associated re-adjustment to a new virial equilibrium provide an attractive way to explain differences between the scaling relations of dwarf and giant ellipticals. We consider this theory more promising than other mechanisms such as dissipation, merging, or tidal stripping of disk galaxies, since these do not appear capable of moving galaxies in the direction of the region that dwarfs occupy in surface brightness and velocity dispersion parameter space (e.g., Bender & Nieto 1990; Bender *et al.* 1992; De Rijcke *et al.* 2005). Hence, we use the predictions of galactic wind models from DS86 and YA87 to test this scenario against the trends seen in our data.

The models of DS86 describe gas loss from self-gravitating systems with similar age and initial stellar mass function. If the galaxy's dynamics are dominated by a dark matter halo, they predict $L \propto \sigma^{5.26}$ and $M/L \propto L^{-0.37}$, leading to $M/L \propto M^{-0.59} \propto \sigma^{-1.95}$. If instead the galaxies contain only baryonic matter and have roughly constant M/L (because of the similar stellar content), they find that after gas loss, dwarfs should adhere to $L \propto \sigma^{2.7}$. YA87 provide a finer level of distinction with two different rates of gas expulsion: slow and rapid. Such models specify a fraction of the galaxy's gas mass to be blown out, the time-scale on which it happens, and the new galaxy structure from the resulting virial equilibrium (although in the case of rapid gas removal, equilibrium is not necessarily reached). For dwarf galaxies that have undergone a complete course of slow, adiabatic gas removal, they obtain $L \propto \sigma^{2.5}$ and mass-to-light ratios that scale inversely with luminosity. However, it should be noted that these scaling relations only apply to the end stage of gas removal; if not all dwarf galaxies have reached this point, then a substantial scatter in their properties might be expected, as suggested by Figure 9 of YA87. De Rijcke *et al.* (2005) overlay a number of late-type galaxies on these galactic wind models, showing a consistency between the positions of dwarf ellipticals, and models including gas removal.

Our data indicate a slow positive trend of M/L with velocity dispersion, of the form $M/L \propto \sigma^{0.19}$. Whilst

this is in broad agreement with the galactic wind models discussed above, it is very different from results from giant galaxies. For giants, the exponents in the range 0.66 to 1.4 have been found in the optical (Jørgensen *et al.* 1996,1998; Guzmán, Lucey & Bower 1993) and the near infra-red (Mobasher *et al.* 1999). It is also different from the trend found for the much lower luminosity local group dwarfs. There Peterson & Caldwell (1993) find $M/L \propto L^{-0.40 \pm 0.06}$ which, together with their measured relation $L \propto \sigma^{5.6 \pm 0.9}$, yields $M/L \propto \sigma^{-2.2 \pm 0.5}$.

Several recent studies have suggested a large variation of slope in the $M/L - \sigma$ relation over many orders of magnitude in galaxy luminosity. From data on a number of clusters, Zaritsky, Gonzalez & Zabludoff (2006) have revealed a dependence that is roughly parabolic and not well represented by a power law. Their trend of M/L on σ becomes flat near $\log \sigma = 1.7$ and is very consistent with our result of $M/L \propto \sigma^{0.19}$ obtained for galaxies with dispersions in that regime. Desroches *et al.* (2007) also find significant curvature in the $M/L - \sigma$ relation among a large set of galaxies from the Sloan Digital Sky Survey, although their sample primarily encompasses objects with significantly larger luminosities and velocity dispersions than our dwarf data. Cappellari *et al.* (2006) have calculated M/L values based on dynamical models of the SAURON galaxy sample (Bacon *et al.* 2001) and conclude that non-homology effects play only a small role in setting the fundamental scaling relations among late-type galaxies; stellar population effects and dark matter properties must instead account for changing mass-to-light ratios.

6 CONCLUSIONS

We have presented velocity dispersions for a sample of 69 dwarf and giant galaxies in the Coma cluster, of which 62 are either elliptical or S0 galaxies in their morphology. We find that the fundamental parameters of low-luminosity ellipticals vary fairly tightly with the velocity dispersion. The relationship between luminosity and velocity dispersion at the boundary of the dwarf and giant regime is clearly different from the classical Faber-Jackson relation for giant elliptical galaxies. The correlation between surface brightness and velocity dispersion in our sample is also very tight and can be explained by observational error in the velocity dispersions alone. There is evidence that the mass-to-light ratio varies systematically along this correlation, with the higher surface brightness galaxies having higher (M/L). We have investigated whether gas removal by galactic winds can explain these results and find that it provides a satisfactory origin for the $L - \sigma$ relation and a possible basis for the trend in mass-to-light ratio.

ACKNOWLEDGMENTS

The WIYN Observatory is a joint facility of the University of Wisconsin-Madison, Indiana University, Yale University, and the National Optical Astronomy Observatories. A.M.C. acknowledges the AAO Student Fellowship Program for support of this work. We would like to thank Pat Knezek and Megan Sosey for help with the observations, as well as WIYN Hydra Instrument Scientist Diane Harmer for assistance with observing preparations. We thank the anonymous referee for helpful comments.

REFERENCES

- Aaronson M. 1983 ApJ, 266, 11
 Arimoto N., Yoshii Y. 1987 A&A, 173, 23
 Bacon R., et al. 2001 MNRAS, 326, 23
 Baum W. A., Hammergren M., Thomsen B., Groth E. J., Faber S. M., Grillmair C. J., Ajhar E. A. 1997 AJ, 113, 1483
 Bender R., Nieto J.-L. 1990 A&A, 239, 97
 Bender R., Burstein D., Faber S. M. 1992 ApJ, 399, 462
 Bernstein G. M., Nichol R. C., Tyson J. A., Ulmer M. P., Wittman D. 1995 AJ, 110, 1507
 Binggeli B., Sandage A., Tarenghi M. 1984 AJ, 89, 64
 Cappellari M. et al. 2006 MNRAS, 366, 1126
 Cappellari M., Emsellem E. 2004 PASP, 116, 138
 Carter D., et al. 2002 ApJ, 567, 772
 Davies R. L., Efstathiou G., Fall S. M., Illingworth G., Schechter P. L. 1983 ApJ, 266, 41
 De Rijcke S., Michielsen D., Dejonghe H., Zeilinger W. W., Hau G. K. T. 2005 A&A 4338, 491
 de Vaucouleurs G. 1948 Ann. d'Astrophysique, 11, 247
 Dekel A., Silk J. 1986 ApJ, 303, 39
 Desroches L.-B., Quataert E., Ma C.-P., West A. 2007 MNRAS, 377, 402
 Djorgovski S., Davis M. 1987 ApJ, 313, 59

- D'Onofrio M., Valentinuzzi T., Secco L., Caimmi R., Bindoni D. 2006 *NewAR*, 50, 447
- Dressler A., Lynden-Bell D., Burstein D., Davis R. L., Faber S. M., Terlevich R., Wegner G. 1987 *ApJ*, 313, 42
- Edwards S. A., Colless M. M., Bridges T. J., Carter D., Mobasher B., Poggianti B. M. 2002 *ApJ*, 567, 178
- Faber S. M., Jackson R. E. 1976 *ApJ*, 204, 668
- Ferguson H. C., Binggeli B. 1994 *A&AR*, 6, 67
- Fish R. A. 1964 *ApJ*, 139, 284
- Geha M., Guhathakurta P., van der Marel R. P. 2002 *AJ*, 124, 3073
- Geha M., Guhathakurta P., van der Marel R. P. 2003 *AJ*, 126, 1794
- Godwin J., Metcalfe N., Peach J. V. 1983 *MNRAS*, 202, 113
- Graham A., Guzmán R. 2003 *AJ*, 125, 2396
- Guzmán R., Lucey R., Bower R. 1993 *MNRAS*, 265, 731
- Held E. V., de Zeeuw P. T., Mould J. R., Picard A. 1992 *AJ*, 103, 851
- Held E. V., Mould J. R., Freeman K. C., 1997, in Arnaboldi, M., da Costa, G. S., Saha, P., eds, *ASP Conf. Ser.* Vol. 116, *The Nature of Elliptical Galaxies*. *Astron. Soc. Pac.*, San Francisco, p.292
- Jørgensen I., Franx M. 1994 *ApJ*, 433, 553
- Jørgensen I., Franx M., Kjaergaard P. 1996 *MNRAS*, 280, 167
- Jørgensen I., Franx M., Hjorth J., van Dokkum P. 1999 *MNRAS*, 308, 833
- Jørgensen I. 1999 *MNRAS*, 306, 607
- Komiyama Y. et al. 2002 *ApJS*, 138, 265
- Kormendy J. 1985 *ApJ*, 295, 73
- Kroupa P. 1998 *MNRAS*, 300, 200
- Mateo M., 1998, in Richtler T., Braun J. M., eds, *Proc. Bonn/Bochum-Graduiertenkolleg Workshop, The Magellanic Clouds and Other Dwarf Galaxies*. *Shaker Verlag, Aachen*, p. 53
- Matković A., Guzmán R. 2005 *MNRAS*, 362, 289
- Matković A., Guzmán R. 2007 *RevMexAA*, 29, 107
- Mobasher B. et al. 2001 *ApJS*, 137, 279
- Mobasher B., Guzmán R., Aragó-Salamanca A., Zepf S. 1999 *MNRAS*, 304, 225
- Moore B., Katz N., Lake G. 1996 *ApJ*, 457, 455
- Nieto J.-L., Bender R., Davoust E., Prugniel P. 1990 *A&A*, 230, L17
- Peterson R. C., Caldwell N. 1993 *AJ*, 105, 1411
- Poggianti B.M. et al. 2001a *ApJ*, 562, 689
- Poggianti B. M. et al. 2001b *ApJ*, 563, 118
- Poggianti B. M., Kashikawa N., Bridges T. J., Mobasher B., Komiyama Y., Carter D., Okamura S., Yagi M. 2004 *ApJ*, 601, 197
- Richstone D. O., Tremaine S. 1986 *AJ*, 92, 72
- Schaeffer R., Silk J. 1988 *A&A*, 203, 273
- Sérsic J. L., 1968, *Atlas de Galaxias Australes*. *Observatorio de Córdoba, Argentina*
- Simien F., Prugniel Ph., 2002 *A&A*, 384, 371
- Smith R. J. et al. 2004 *AJ*, 128, 1558
- Smith R. J. et al. 2008 *MNRAS*, 386, L96
- Tonry J., Davis M. 1979 *AJ*, 84, 1511
- Valdes F., Gupta R., Rose J., Singh H., Bell D. 2004 *ApJS*, 152, 251
- van Zee L., Skillman E. D., Haynes M. P. 2004 *AJ*, 128, 121
- White S. D. M., Frenk C. S. 1991 *ApJ*, 379, 52
- Wilkinson M. I., Kleyna J., Evans N. W., Gilmore G. 2002 *MNRAS*, 330, 778
- Yoshii Y., Arimoto N. 1987 *A&A*, 188, 13
- Zaritsky D., Gonzalez A., Zabludoff A. 2006 *ApJ*, 638, 725

APPENDIX A: VELOCITY AND VELOCITY DISPERSION DATA

Table A1: Velocities and velocity dispersions of Coma dwarfs

GMP ID	Komiyama ID	Type	RA (J2000)	Dec (J2000)	Kron R mag.	B-R mag.	$\mu_{R,eff}$ mag/('') ²	cz km s ⁻¹	Error km s ⁻¹	σ km s ⁻¹	Error km s ⁻¹	S/N (per Å)
4644	48397	dE	12 58 34.1	26 53 60	18.17	1.37	21.63	8103	5	6	4	7.0
5361	50320	E	12 56 36.0	26 54 18	16.44	1.42	20.97	7886	4	39	4	13.7
4518	55692	E	12 58 03.2	26 54 58	14.51	1.41	19.30	8203	6	70	4	16.6
4340	53772	E/S0	12 58 20.3	26 55 14	16.93	1.24	20.59	6934	3	31	3	20.9
4418	59497	dE	12 58 13.0	26 56 59	18.02	1.47	21.74	6732	6	21	5	7.0
4980	65832	E/S0	12 57 18.6	26 58 47	17.46	1.42	21.27	7293	4	34	4	12.0
5395	83625	S0	12 56 32.0	27 03 21	14.81	1.37	18.87	6143	8	122	5	28.6
5259	82181	dS0	12 56 47.1	27 03 25	17.57	1.22	22.18	6490	8	21	5	6.6
5097	87820	dE	12 57 05.8	27 05 21	18.23	1.50	22.44	7478	5	12	4	7.4
5032	92047	S0	12 57 12.0	27 06 13	16.03	1.40	20.85	7331	4	47	3	17.7
4135	103965	SBc	12 58 37.3	27 10 35	14.82	1.06	19.84	7654	9	42	3	33.3
5365	115034	S0/a	12 56 34.6	27 13 40	15.28	1.25	20.79	7188	4	44	3	20.0
4591	113838	E	12 57 55.4	27 13 55	17.28	1.37	21.27	6469	4	21	4	12.0
5422	130251	Sc/SBc	12 56 28.6	27 17 29	14.67	1.15	21.28	7522	4	37	3	22.3
4351	131621	S0pec	12 58 18.7	27 18 38	15.77	1.18	20.36	7410	17	54	3	21.6
4565	138413	dE	12 57 58.0	27 21 03	18.02	1.46	21.00	8672	5	33	4	11.5
5364	144552	SB0	12 58 33.1	27 21 52	14.82	1.55	20.31	7009	5	84	4	21.6
5136	143923	SB0	12 57 01.7	27 22 20	15.18	1.52	20.03	7004	5	95	4	22.9
4375	145796	E	12 57 56.5	27 22 56	16.54	1.48	21.13	5221	3	27	4	14.7
4215	149036	dS0	12 58 31.7	27 23 42	17.48	1.29	21.98	7571	5	7	4	9.9
4479	153508	E/S0	12 58 06.1	27 25 08	16.00	1.43	20.75	5774	3	45	3	18.1
5250	154595	S0	12 56 47.8	27 25 16	15.64	1.40	20.12	7777	3	46	3	23.2
4430	156329	E/S0	12 58 20.5	27 25 46	16.61	1.319	20.69	7540	3	38	3	22.3
5526	161876	E/SB0	12 56 16.7	27 26 45	14.89	1.71	19.76	6404	8	112	5	25.1
5296	159473	S0	12 56 40.9	27 26 52	17.32	1.50	20.69	7338	3	43	3	17.2
4381	162274	dE/S0	12 58 15.3	27 27 53	17.62	1.52	21.17	7650	6	22	4	7.9
4956	164198	E	12 57 21.7	27 28 30	16.98	1.69	20.13	6942	4	50	3	15.9
4597	169748	SBc	12 57 54.4	27 29 26	15.02	1.36	21.09	4986	4	65	3	24.5
4522	167048	E	12 57 50.8	27 29 27	17.31	1.47	20.10	7341	4	55	3	16.4
5102	180920	S0	12 57 04.3	27 31 34	15.97	1.47	20.62	8341	3	42	3	18.3
4852	176486	E	12 57 30.6	27 32 35	16.61	1.60	19.95	7653	4	64	3	21.5
4117	180017	E	12 58 38.4	27 32 39	15.15	1.54	19.19	5986	7	108	5	26.1
5284	181166	S0	12 56 42.4	27 32 54	16.54	1.47	20.41	7571	3	51	3	20.9
3760	2623	dE	12 59 6.38	27 33 39	17.86	1.48	22.43	7767	6	16	5	6.0
3271	5443	S0/a	12 59 39.8	27 34 36	15.51	1.02	20.42	4997	5	26	3	32.1
3585	6728	S0	12 59 18.5	27 35 37	16.77	1.16	21.65	5216	5	21	4	19.9
3598	13606	dE	12 59 17.1	27 38 03	17.99	1.51	21.72	5282	5	38	4	9.8
2801	23231	dS0	13 00 17.4	27 42 41	17.89	1.57	21.54	7108	5	22	4	9.1
3586	23987	E	12 59 18.3	27 42 56	16.68	1.58	20.36	6679	3	46	3	20.7
3176	28211	S0	12 59 46.3	27 44 46	17.26	1.09	21.52	9718	7	42	4	14.6
4035	29543	E	12 58 45.5	27 45 14	16.97	1.50	21.77	6646	4	26	4	12.0
4150	31541	dE	12 58 35.4	27 46 30	18.60	1.41	22.06	5956	6	17	5	6.0
2478	39218	E/S0	13 00 45.4	27 50 08	16.53	1.59	20.76	8800	3	41	3	20.4
4175	39682	E/S0	12 58 33.8	27 50 12	17.08	1.36	21.02	4486	5	35	5	8.9
2753	41046	E/S0	13 00 20.2	27 50 36	16.53	1.60	20.92	7856	3	37	3	16.9
3473	42068	dE	12 59 26.4	27 51 25	17.68	1.54	21.36	4967	5	33	4	10.1
3645	46757	E	12 59 14.6	27 53 44	17.30	1.59	20.26	6409	6	57	5	11.7
2736	47098	E	13 00 21.6	27 53 55	16.74	1.49	20.79	4896	3	35	3	17.5
2376	47923	S0	13 00 55.9	27 53 55	16.69	1.60	21.89	6010	4	31	4	11.1
3080	49731	dE	12 59 55.7	27 55 03	18.07	1.72	21.75	6668	3	16	4	8.6
3511	50139	cE	12 59 23.4	27 55 10	17.27	1.66	19.56	6923	6	95	4	23.9
3376	50554	dE	12 59 32.0	27 55 15	17.66	1.49	22.01	7079	4	28	4	12.3
2692	52689	S0/a	13 00 24.8	27 55 36	16.78	1.62	21.39	7972	3	44	3	17.1
3565	57356	E/S0	12 59 19.7	27 58 24	17.04	1.53	21.49	7247	4	32	4	13.9
3602	58030	dE	12 59 16.7	27 58 57	19.02	1.58	21.71	6878	5	13	4	6.9
3018	59516	dE	13 00 01.0	27 59 30	18.08	1.62	21.86	7549	6	20	4	7.4
3166	59610	E	12 59 46.9	27 59 31	17.36	1.46	21.58	8410	4	35	4	12.4
3292	60593	S0/a	12 59 38.0	28 00 03	16.62	1.51	20.96	4980	3	43	3	18.4
3969	61500	E	12 58 50.8	28 00 25	17.36	1.55	21.30	7460	3	21	4	14.7
3681	62166	E	12 59 11.5	28 00 33	16.70	1.50	20.72	6895	3	48	3	20.3
4042	63244	SB0	12 58 48.1	28 01 07	17.03	1.64	21.91	7116	5	25	5	7.6
2879	68886	E	13 00 11.1	28 03 55	16.67	1.52	20.90	7350	4	46	3	20.4
3387	72587	E	12 59 31.6	28 06 02	17.29	1.42	21.92	7427	4	33	4	12.3
2976	79519	S0	13 00 04.2	28 09 18	16.63	1.49	20.81	6586	3	40	3	17.4
3699	81862	S0/Sp	12 59 09.9	28 09 52	17.36	1.35	21.57	8612	5	28	4	12.3
3204	82303	E	12 59 44.1	28 10 35	16.98	1.54	20.58	8316	3	42	3	18.1
4122	86791	dE	12 58 37.4	28 13 10	17.61	1.55	21.68	6784	5	31	5	9.2
3640	90411	E/S0	12 59 15.0	28 15 03	16.60	1.00	21.47	7428	4	23	3	21.2
3902	104960	dE	12 58 55.8	28 21 14	18.09	1.63	22.16	6355	6	15	5	6.7